

Review of passive imaging polarimetry for remote sensing applications

J. Scott Tyo, Dennis L. Goldstein, David B. Chenault, and Joseph A. Shaw

Imaging polarimetry has emerged over the past three decades as a powerful tool to enhance the information available in a variety of remote sensing applications. We discuss the foundations of passive imaging polarimetry, the phenomenological reasons for designing a polarimetric sensor, and the primary architectures that have been exploited for developing imaging polarimeters. Considerations on imaging polarimeters such as calibration, optimization, and error performance are also discussed. We review many important sources and examples from the scientific literature. © 2006 Optical Society of America
OCIS codes: 110.0110, 120.0280, 120.5410.

1. Introduction and Background

A. Overview

The primary physical quantities associated with an optical field are the *intensity*, *wavelength*, *coherence*, and *polarization*. Conventional panchromatic cameras measure the intensity of optical radiation over some wave band of interest. Spectral imagers measure the intensity in a number of wave bands, which can range from one or two (three is common for a color camera) through multispectral systems that measure of the order of 10 spectral channels to hyperspectral systems that may measure 300 spectral channels or more. Spectral sensors tend to give us information about the distribution of material components in a scene. Polarimetry seeks to measure information about the vector nature of the optical field across a scene. While the spectral information tells us about

materials, polarization information tells us about surface features, shape, shading, and roughness. Polarization tends to provide information that is largely uncorrelated with spectral and intensity images, and thus has the potential to enhance many fields of optical metrology. Figure 1 shows one example of the ability of polarization to show enhanced contrast when there is little contrast in intensity imagery.

Imaging polarimetry is a special case of general polarimetry that is dedicated to mapping the state of polarization across a scene of interest. Applications of polarization imagery range from remote sensing to microscopy to industrial monitoring. All the concerns of general polarimetry apply; i.e., a measurement method still has to be chosen and calibration must be performed, but now the additional issues associated with measuring a 2D region in space exist. Sequential or simultaneous images must be registered, and we must know that the response of individual detectors is linear and, if multiple detectors are used, uniform in response with respect to all other detectors.

In this paper, we provide what we believe is the first in-depth review of the progress that has been made specifically in the field of imaging optical polarimetry for remote sensing. Most of the work discussed here has been carried out over the past three decades. Our focus is on *imaging*, so there are many important references on ellipsometry and other forms of nonimaging polarimetry that are omitted here because of scope. Our primary focus is on passive Stokes-vector imagers, though we do discuss some of the very recent work that is beginning to emerge in active Mueller matrix imagers and polarization lidar. Where possible, we refer to the earliest source known

When this research was performed, J. S. Tyo (tyo@ieee.org) was with the Department of Electrical and Computer Engineering, University of New Mexico, Albuquerque, New Mexico 87131. He is now with the College of Optical Sciences, University of Arizona, Tucson, Arizona 85721. D. L. Goldstein (dennis.goldstein@eglin.af.mil) is with the U.S. Air Force Research Laboratory/MNGI, Eglin Air Force Base, Florida 32542. D. B. Chenault (david@polarissensor.com) is with Polaris Sensor Technologies, Incorporated, 200 West Side Square, Suite 320, Huntsville, Alabama 35801. J. A. Shaw (jshaw@ece.montana.edu) is with the Department of Electrical and Computer Engineering, Montana State University, Bozeman, Montana 59717.

Received 17 November 2005; revised 4 April 2006; accepted 6 April 2006; posted 10 April 2006 (Doc. ID 66019).

0003-6935/06/225453-17\$15.00/0

© 2006 Optical Society of America

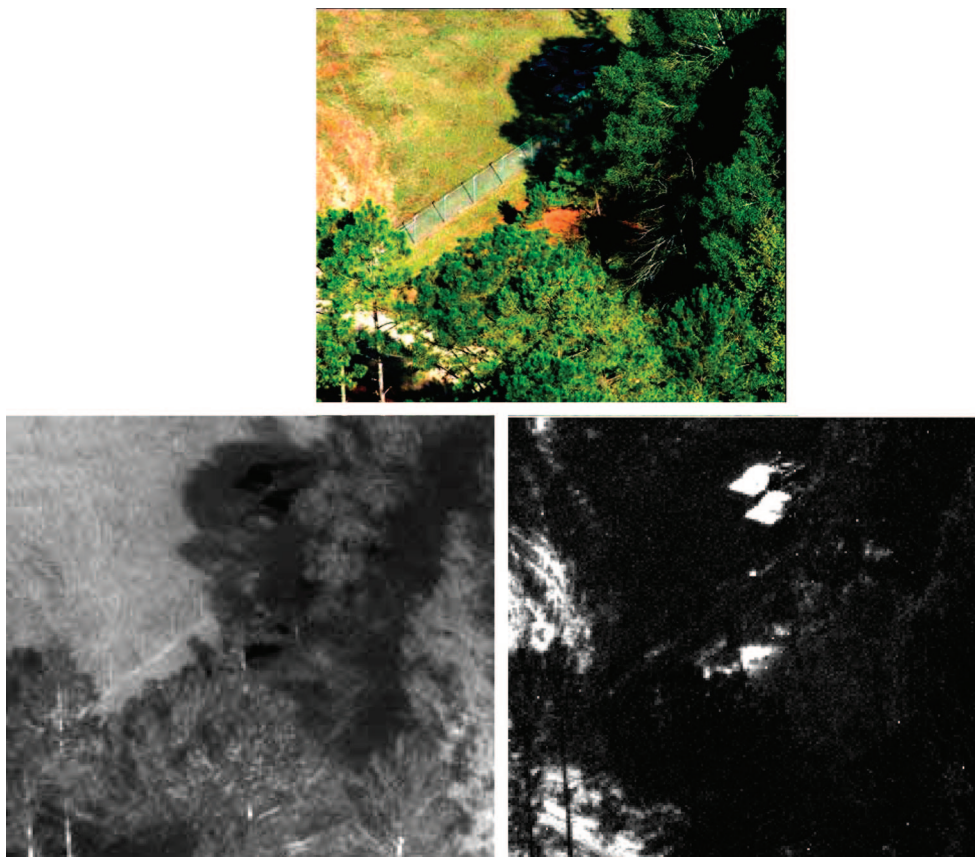


Fig. 1. (Color online) Visible picture of two pickup trucks in the shade (top), long-wave IR intensity image (bottom left), and long-wave IR polarization image (bottom right). Strong contrast in the polarization image shows advantages for enhanced target detection using imaging polarimetry. (Courtesy of Huey Long, U.S. Army Research Laboratory, Adelphi, Maryland.)

to us, preferably from the reviewed scientific literature.

In this introductory section, we offer a set of definition of terms that are used in the paper, as well as a brief historical perspective. Section 2 describes the phenomenology of imaging polarimetry, and Section 3 describes types of measurements and data reduction techniques. In Section 4, we give general measurement strategies that have been used, and in Section 5, a discussion of systems engineering issues. Finally, conclusions are presented in Section 6.

B. Definition of Terms

Angle of polarization: the angle of the major axis of the polarization ellipse with respect to the x axis. Mathematically in terms of the Stokes-vector elements,

$$\psi = \frac{1}{2} \arctan \frac{s_2}{s_1}. \quad (1)$$

Depolarization: the process of changing polarized light into unpolarized light.

Diattenuation: a property of a polarization element that describes the intensity contrast ratio between orthogonal transmitted polarization states.

Degree of circular polarization (DOCP): the fraction of the intensity attributable to circular polarized light states. Mathematically in terms of the Stokes-vector elements,

$$\text{DOCP} = s_3/s_0. \quad (2)$$

Degree of linear polarization (DOLP): the fraction of the intensity attributable to linear polarized light states. Mathematically in terms of the Stokes-vector elements,

$$\text{DOLP} = \sqrt{s_1^2 + s_2^2}/s_0. \quad (3)$$

Degree of polarization (DOP): the fraction of the intensity attributable to polarized light states. Mathematically in terms of the Stokes-vector elements,

$$\text{DOP} = \frac{\sqrt{s_1^2 + s_2^2 + s_3^2}}{s_0}. \quad (4)$$

Division of amplitude polarimeter (DoAmP): a polarimeter that makes measurements by splitting the light into different optical paths, each with distinct

polarization optics, and using a separate focal-plane array to image each path.

Division of aperture polarimeter (DoAP): a polarimeter that uses a lens array to focus separate parts of the aperture onto separate focal-plane arrays or subarrays. Each subarray measures a different polarization state.

Division of focal-plane polarimeter (DoFP): a polarimeter that uses a micro-optical array of polarization elements to make different polarization measurements at each pixel on the focal-plane array.¹

Imaging polarimetry: the process of measuring polarization properties of light, an element, or a system so as to build an extensive 2D description of the polarization properties, ordinarily recognized as a picture by a human observer.

Jones² formalism: the mathematical method of describing polarized light in terms of amplitudes and phases. Devised by Jones, light is represented by a two-element (Jones) vector of complex numbers. A polarization element or system is described by a 2×2 (Jones) matrix of complex numbers. All Jones' matrices represent elements that can be realized in hardware, but not all elements that can be realized in hardware can be represented by a Jones matrix.

Lu–Chipman³ decomposition: a method of interpreting the Mueller matrix as a factorable product of a diattenuator matrix, a retarder matrix, and a depolarizer matrix.

Mueller matrix: the 4×4 real matrix representing the properties of an optical element or system in the Mueller–Stokes formalism. The matrix is often normalized to the (1, 1)th entry so that the values range from +1 to -1. This normalization is then in terms of the unpolarized scattering of the system.

Poincaré sphere: representation of light polarization states as points on a sphere. The coordinates of a point on the Poincaré sphere corresponds to the three Stokes-vector elements s_1 , s_2 , and s_3 .

Polarizance⁴: the degree of polarization produced by a polarizer when the incident beam is unpolarized. Polarizance is a property of the polarization element.

Polarization state analyzer⁵ (PSA): a collection of retarders and linear polarizers cascaded to form an elliptical diattenuator used for analyzing an unknown incident Stokes vector.

Polarization state generator⁵ (PSG): a polarization state analyzer used in reverse to create an arbitrary elliptical polarization state.

Retardance: the change of phase introduced by an element or system between two states of polarization in a beam of light.

Spectropolarimetry: the process of measuring the polarization properties of light, an element, or a system over some defined spectral region.

Stokes⁶ vector: a four-element real vector describing polarized or partially polarized light, based on intensity measurements. Introduced by Stokes in 1852, it can describe partially polarized light. We use the symbols s_0 , s_1 , s_2 , and s_3 for the four Stokes-vector elements defined as

$$\mathbf{S} = \begin{bmatrix} s_0 \\ s_1 \\ s_2 \\ s_3 \end{bmatrix} = \begin{bmatrix} \langle |E_x|^2 + |E_y|^2 \rangle \\ \langle |E_x|^2 - |E_y|^2 \rangle \\ 2 \operatorname{Re} \langle E_x E_y^* \rangle \\ -2 \operatorname{Im} \langle E_x E_y^* \rangle \end{bmatrix} \propto \begin{bmatrix} I_0 + I_{90} \\ I_0 - I_{90} \\ I_{45} - I_{135} \\ I_L - I_R \end{bmatrix}. \quad (5)$$

In Eq. (5), s_0 is the total intensity of the light, s_1 is the difference between horizontal and vertical polarization, s_2 is the difference between linear $+45^\circ$ and -45° polarization, and s_3 is the difference between right and left circular polarization. These elements are often normalized to the value of s_0 so that they have values between +1 and -1.

C. Historical Perspective

Someone peering through a birefringent crystal and observing a pair of refracted polarized images probably did the earliest imaging polarimetry. There are two important early experiments by Arago and Fresnel,⁷ Arago,⁸ and Millikan^{9,10} that are often reported as the earliest attempts at quantitative polarimetry. Arago performed a number of qualitative experiments involving polarized light, and was the first to observe the phenomena of optical activity and that emitted radiation is not always unpolarized. Millikan measured the linear polarization information from incandescent molten metals, and there were a number of subsequent studies that explored polarization of emitted radiation. Sandus¹¹ provides a thorough review of the physics and these early works.

To discuss imaging polarimetry in the modern quantitative sense, we must leap forward to the age of solid-state electronics. The earliest work known to us is contained in two originally classified government reports, the first by Johnson¹² in 1974 and the second by Chin-Bing¹³ in 1976. The instrument described in these reports is a thermal infrared scanning camera that was modified by adding a second detector and a polarizing prism. A 1976 patent by Garlick *et al.*,¹⁴ described a system that displayed a differential optical polarization image. The earliest publications describing imaging polarimetry in the visible are the papers by Walraven^{15,16} where a linear polarizer was rotated in front of a film camera. The developed film was digitized, and linear Stokes-vector elements calculated. Solomon¹⁷ gave an early review of imaging polarimetry in 1981. Polarimetric sensors also have been used on manned and unmanned spacecraft. Pioneer 11 has the Imaging Photopolarimeter on board,¹⁸ and the space shuttle has carried dual film cameras¹⁹ and later three-color digital cameras with polarization optics²⁰ operated by a mission specialist. These systems measured two or three components of linearly polarized light. Three cameras were used by Prosch *et al.*²¹ to obtain the first three Stokes-vector elements, and dual piezoelectric modulators were used by Stenflo and Povel²² to measure the full-Stokes vector. Pezzaniti and Chipman^{23,24} developed a Mueller matrix imaging polarimeter that has been used to examine optical elements in transmission and reflection. There are many other exam-

Table 1. Polarization Phenomenology and Effects from the Visible to the LWIR

	Advantages	Disadvantages
Visible, NIR, SWIR Typical signal: 1%–60% Sensor resolution: >1%–2%	<ul style="list-style-type: none"> • Sun is a strong source • High dynamic range of polarization signatures • Sensors cheaper, easier to build and calibrate 	<ul style="list-style-type: none"> • Strongly dependent on geometry • High dynamic range of signatures • Inconsistent signatures • Small well size for FPAs limits polarimetric resolution • No night operation
MWIR Typical signal: 0.1%–25% Sensor resolution: >0.2%	<ul style="list-style-type: none"> • Good signatures for hot targets • Night operation • Large well sizes for FPA for better sensitivity 	<ul style="list-style-type: none"> • Signatures combination of emissive and reflective • Sensors require cooling • Sensors more expensive and difficult to build and calibrate
LWIR Typical signal: 0.1%–20% Sensor resolution: <0.1%	<ul style="list-style-type: none"> • Signatures dominated by emission • Less dynamic range for polarization signatures • Large well sizes for FPA for better sensitivity • Night operation 	<ul style="list-style-type: none"> • Sensors require cooling • Sensors most expensive and difficult to build and calibrate

ples. The sources cited are each early realizations of a particular type of imaging instrument.

2. Measurement Considerations

The basic aspects of light that are typically measured in imaging scenarios are intensity, spectral content, coherence, and polarization. For passive imaging polarimetry, it is often most convenient to represent the polarization information in terms of the Stokes vector, which is defined in terms of the time-averaged intensity as in Eq. (5). Implied in Eq. (5) is that the intensity measurement is made over some spectral range. The range could be broad or narrow, and the choice of spectral bands is discussed in Subsection 2.A.

A. Spectral Considerations

Spectral information usually tells the observer something about the molecular makeup of the materials that compose a scene. Multispectral and hyperspectral imagers have been developed to exploit this class of information.²⁵ While there are exceptions, polarization information is a slowly varying function of wavelength,^{26–28} so it provides information that tends to be uncorrelated with any spectral measurements that are made in a system.

When pursuing a particular application of imaging polarimeters, spectral considerations are among the first issues to be addressed. There are advantages and disadvantages in each spectral band as in intensity imaging both from the consideration of detection instrumentation as well as the phenomenology the user is trying to exploit. Imaging polarimeters typically are based on silicon in the visible (VIS) to near-infrared (NIR) spectra, may use InGaAs in the short-wave infrared (SWIR), InSb in the midwave infrared (MWIR), and HgCdTe in the long-wave infrared (LWIR). The characteristics of these detector types that are considered when used in nonimaging systems apply to imaging polarimeters as well, i.e., silicon-based imagers are inexpensive relative to IR systems, IR systems must be cooled but have day and/or night capability, etc.

In terms of the phenomenology, polarization signatures in the visible and NIR parts of the spectrum are dominated by reflection. Thus these signatures depend on an external source for illumination, primarily the Sun. The polarization has a wide dynamic range and can show rapid spatial variation when imaging outdoor scenes. The measured polarization information is dependent on source–scene–sensor geometry, and therefore can vary significantly depending on the time of day or sensor location. In the MWIR, polarization signatures are a combination of both reflected and emitted radiation, which tend to cancel or reduce the overall degree of polarization. In the LWIR, the signatures are dominated by emission and can be very stable in time when scene temperatures are stable. Unfortunately, in the LWIR, spatial resolution is reduced and the cost and complexity of building a system are generally increased.

In outdoor measurements, the most rapid variations of polarization with wavelength result from atmospheric spectral features.²⁶ In the VIS–NIR–SWIR, there is strong variation with atmospheric aerosol content. The MWIR contains significant emitted and reflected terms, and LWIR scenes depend strongly on atmospheric water vapor. Some of the issues that arise for imaging polarimetry with respect to spectral regions are given in Table 1.

B. One-Dimensional Polarimeters

The simplest possible use of polarimetry in imaging is to put a polarization analyzer in front of a camera and to adjust the polarization state of this polarizer to maximize the contrast between an object and its background. This is a common technique used in photography, for example, when taking a picture of an object against linearly polarized skylight. Similar techniques have been used in underwater imagery to mitigate the effect of scattering using both linear²⁹ and circular³⁰ polarization analyzers with both unpolarized and polarized illumination. The light scattered by the medium may have a preferred polarization state owing to the polarization of the source and the illumi-

nation geometry. The general strategy is to select a polarization analyzer that is orthogonal to the polarization state of the background or haze.

C. Two-Dimensional Polarimeters

The natural extension of the 1D polarization imager is a polarization difference imager that measures the intensity of light at two polarization states, then adds them to estimate s_0 and subtracts them to estimate s_1 , s_2 , or s_3 , or some linear combination thereof. Simple 2D imagers have shown applicability in a number of scenarios, but are most widely used in clutter rejection²⁸ and in mitigating the effects of random media.^{31–36} The basic assumption in these cases is that there is a difference between the polarization properties of light coming from the background and the light coming from a target. In such cases, significant contrast enhancement can be obtained.

Two-dimensional polarimetry has been used with both unpolarized^{28,31} and polarized^{30,32,33,37} illumination. Two-dimensional polarization discrimination has been widely used in scattering media, and has been shown to increase the range at which targets can be detected by a factor of 2 to 3.^{31,32} When used with passive or quasi-passive systems, polarization imaging has been shown to penetrate as much as five to six photon mean-free paths into random media. For time-gated imagery, polarization can allow penetration to greater than ten photon paths.^{33,38} The improved performance of differential polarimetry over conventional imagery in scattering media can be directly attributed to the depolarizing effect of multiple scattering. This results in a spatially narrower point spread function for differential polarization imagery than for intensity imaging.³⁹ In time-gated imagery, there is a clear temporal dependence of the degree of polarization of scattered light that can be used to refine the time gate and mitigate the effect of scatterers.^{37,40}

D. Three-Dimensional Polarimeters

The most common class of imaging polarimeter that has been developed is the linear polarization imager designed to measure s_0 , s_1 , and s_2 . In most passive imaging scenarios, there is very little expected circular polarization. Since the most complicated Stokes parameter to measure is s_3 , it is often omitted to reduce the cost of the imaging system. Probably the earliest well-known example of a full linear Stokes imaging polarimeter was reported by Walraven,^{15,16} who used linear polarizers and photographic film. Other systems have been developed since that perform full linear polarimetry in all regions of the optical spectrum.

When a fixed-position retarder of variable retardance is combined with a linear polarization analyzer, it is possible to create a 3D Stokes polarimeter that measures s_0 , s_1 , and s_3 as discussed in Section 3.B. Such a system is sensitive to a linear polarization difference and a circular polarization difference, and systems such as these have been used for imaging in scattering media.^{30,32,37}

E. Full-Stokes Polarimeters

In some applications, it is essential to measure all of the available polarization information. For a passive imaging system, this means that the full-Stokes vector must be measured at every pixel in the scene. Solomon¹⁷ provided one of the first early treatments that specifically addressed full-Stokes imaging polarimetry in 1981. Since then, numerous systems have been built that can perform full-Stokes imaging, and we review many of these systems in the rest of the paper organized by the class of spectral imager and the techniques used to perform the measurement.

F. Active Imaging Polarimeters

The primary focus of this review is passive imaging polarimeters that measure the state of polarization of light from an external source. However, it is appropriate to discuss some of the important recent advances in active systems that measure the Mueller matrix or some subset of the Mueller matrix. Similarly, we briefly discuss recent developments in polarization lidar systems, which record backscattered light from a pulsed laser in two or more polarization states as a function of range. In all active polarimeters, the source is known and controlled. The source may generate one or more states of polarization, and the detection system may sense two or more states of polarization. Partial or full measurement of the Stokes vector of the reflected light may be what the sensor is designed for, but in the most complete form of active imaging, the Mueller matrix for each pixel of the illuminated object is obtained. There are two primary forms of active imaging polarimeters. The first are those that create an entire scene in one image collection. The second are lidar systems that scan pixel by pixel to create a scene, and possibly even a volumetric scene with range-gated data.

1. Mueller Matrix and Other Active Imaging Systems

Pezzaniti and Chipman²⁴ and Chipman⁴¹ describe Mueller matrix imaging polarimeters that are used to examine samples in transmission or in reflection. Dual rotating retarders are used in these instruments according to the scheme devised by Azzam.⁴² Cl  menceau *et al.*⁴³ operated a Mueller matrix imaging polarimeter in a monostatic configuration. They also used a dual-rotating-retarder system, but collected only 16 images, the minimum number of measurements needed to determine an arbitrary unknown Mueller matrix. All the systems discussed so far use monochromatic sources. Le Hors *et al.*⁴⁴ showed a system using a white-light source that was spectrally filtered prior to entering the CCD camera. A linear polarizer was placed in front of the source, and two linear polarization states were measured. In this way, images at three colors and two polarization states per color were obtained. Breugnot and Cl  menceau⁴⁵ have set up a system based on Azzam's dual-rotating-retarder configuration using a laser source in a monostatic configuration, but argue that a limited number of Mueller matrix elements are im-

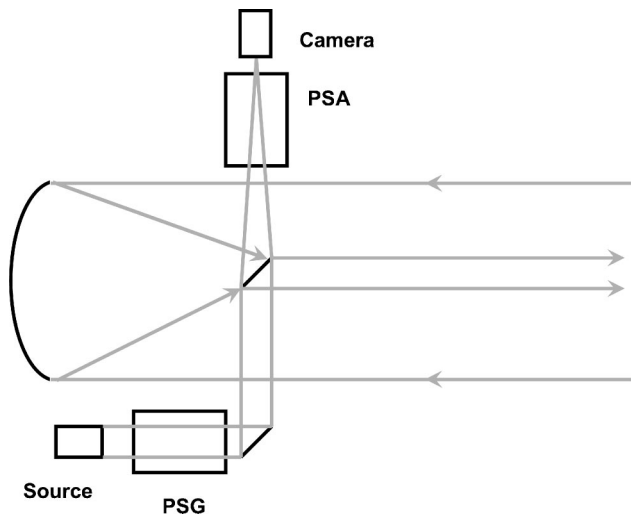


Fig. 2. Experimental setup of the active polarimetric imaging system of Breugnot and Clémenceau in Ref. 45.

portant and these can be obtained with only two measurements. A diagram of such a system is shown in Fig. 2. Réfrégier and Goudail⁴⁶ have also developed contrast parameters of polarization for active imagery and, with others, have looked at the problem of estimating the degree of polarization in active systems.⁴⁷ High-speed Mueller matrix imaging systems for laboratory samples have been described by Baba *et al.*⁴⁸ and by Wolfe and Chipman.⁴⁹ A different technique was introduced by Mujat *et al.*,⁵⁰ that uses interferometric methods with active imagery. If the direction within the Poincaré sphere across an image is uniform and is known or can be assumed, as is sometimes the case with active illumination, then the degree of polarization and retardance can be monitored in a single image.

2. Lidar Systems

Polarization is also found to be useful in more traditional lidar remote sensing. For example, the presence of significant cross-polarized light relative to a linearly polarized transmitter can indicate the presence of ice in clouds or nonspherically shaped dust particles in the atmosphere.^{51–54} Polarized lidars have been developed to measure Stokes parameters of backscattered light in studies of forest and Earth-surface properties,^{55,56} and to enhance contrast in the lidar detection of fish.⁵⁷

Polarization lidar systems typically employ linearly polarized laser transmitters that provide ranging from the round-trip transit time of a backscattered pulse. The polarization selectivity is typically built into the receiver, often using polarization beam splitters to send orthogonally polarized beams to two separate detectors for simultaneous detection of copolarized and cross-polarized scattering. Multiple telescopes can also be used to provide simultaneous measurement of the Stokes parameters of backscattered light.⁵⁵ Lidars have been reported recently that use Pockels cells⁵² or

liquid-crystal variable retarders⁵⁸ to vary the receiver polarization state electronically between laser pulses.

G. Spectropolarimetric Imagers

A spectropolarimetric imager allows the measurement of polarization as a function of wavelength in an imaged scene. When it is not necessary to obtain spectral data rapidly or simultaneously, it is possible to combine a more traditional imaging polarimeter with a rotating filter wheel that selects predetermined spectral bands.⁵⁹ One example application where this kind of system finds use is the study of sky polarization, for which wide angular coverage and rapid polarization measurements are needed, but for which rapid spectral measurements may not be necessary.^{60–63} This approach enjoys relatively simple data retrieval and spectral calibration, but is also slow (in spectral space) and requires moving parts, making it unsuitable for some applications where rapid spectral data are required. Lemke *et al.*⁶⁴ describe a system that uses a combination of rotating filters and polarizers to achieve time-sequential polarization images in an extremely wide wavelength range of 2–240 μm .

Loe and Duggin⁶⁵ described the use of a liquid-crystal tunable spectral filter to electronically tune across multiple 10 nm wide wavelength bands in a system that employed a rotating linear polarizer and a CCD camera to achieve three-Stokes-parameter spectropolarimetric imaging. This was developed as a prototype of a single channel for a four-channel system. Eventually the full system would employ four such systems with a stationary polarization element oriented to provide a full-Stokes image at each wavelength band.

A faster, but still not simultaneous, method of achieving electronic spectral tuning in a spectropolarimeter is to use an acousto-optic tunable filter (AOTF) as a spectral tuning element. The separate ordinary-ray and extraordinary-ray beams from the AOTF can be used to generate two simultaneous images with orthogonal linear polarization. Alternatively, the AOTF can be combined with an external polarizing element (such as a variable retarder) to obtain time-sequential Stokes-vector images.^{66–69} AOTF elements provide rapid spectral tuning with typical delay times of 10–20 ms. An active-spectropolarimeter variation of this approach was described by Prasad,⁷⁰ using a simultaneously tuned AOTF receiver and tunable laser source.

Rather than obtaining multiple spatial dimensions simultaneously and spectral information over time, it is also possible to use one dimension of an imaging array to capture spectral data while using the other array dimension to record 1D spatial data. In this case, a full spectropolarimetric image is built up by spatially scanning the sensor's field of view (FOV) across the scene. For example, Tyo and Turner²⁷ used a polarimeter comprising two liquid-crystal variable retarders and a fixed linear polarizer in combination with a monolithic Fourier transform interferometer to achieve line-scanned spectropolarimetric images of

laboratory test objects. Jensen and Peterson⁷¹ used a complementary strategy of feeding a grating spectrometer by an infrared liquid crystal for imaging polarimetry in the SWIR.

Several related schemes exist for obtaining simultaneous spectropolarimetric images with no moving parts and no temporal delay between spatial, spectral, or polarimetric data. The polarimetric strategy is *channeled spectropolarimetry* discussed in Section 3.C. This “snapshot imaging spectropolarimetry” typically employs birefringent crystals^{72,73} or holographic optical elements⁷⁴ to record fringe patterns from which spectropolarimetric images can be retrieved through a variety of numerical inversion techniques. The obvious advantage is the simultaneous collection of all measured information, but the technique requires intensive computation and is not well suited to images with significant low-spatial-frequency or high-spectral-frequency content.⁷⁴

3. Mathematical Basis for Measurement Techniques

The Stokes vector cannot be directly measured. To create an image of a scene, several individual measurements must be made and then combined to infer the Stokes vector. The measurement strategies can be broadly grouped into three categories: data reduction matrix techniques,⁵ Fourier-based techniques,⁷⁵ and channeled spectropolarimeters.⁷⁶ In this section, we will discuss the general principles of each of these methods.

A. Data Reduction Matrix Techniques

The most straightforward method might be to measure four linearly polarized intensities through a linear analyzer oriented at 0°, 45°, 90°, and 135° and through a left- and right-circular analyzer. The elements could then be combined following the definition of the Stokes vector in Eq. (5). However, the Stokes vector has only four degrees of freedom, and this strategy would entail six measurements. A method has been developed known as the data reduction matrix method⁵ that describes the operation of a polarimeter designed to measure the Stokes vector.

A polarimeter is typically composed of a collection of retarders and polarizers that are cascaded to form a polarization state analyzer (PSA). In general, there may be one or more retarders placed in front of a linear polarizer. The component Mueller matrices are multiplied together to form a general elliptical diattenuator Mueller matrix as³

$$\mathbf{M}_D = T_u \begin{bmatrix} 1 & \bar{D}^T \\ \bar{P} & \sqrt{1-D^2}\mathbf{I}_3 + (1-\sqrt{1-D^2})\mathbf{a}_D\mathbf{a}_D^T \end{bmatrix}. \quad (6)$$

The three-element column vector \bar{D} in Eq. (6) is the *diattenuation vector*³ that gives the location on the Poincaré sphere of the polarization state that passes the diattenuator with maximum intensity. The unit vector \mathbf{a}_D points in the direction of D , and D is the diattenuation of the diattenuator, defined as

$$D = \frac{|T_q - T_r|}{T_q + T_r}, \quad (7)$$

where q and r are the two orthogonal states that are passed with maximum and minimum transmission. When we consider ideal polarization optics, we typically have $|\bar{D}| = 1$, and we can define a diattenuation Stokes vector as

$$\mathbf{S}_D = \begin{bmatrix} 1 & \bar{D}^T \end{bmatrix}^T. \quad (8)$$

When the unknown incident Stokes-vector \mathbf{S}_{in} passes through the diattenuator, the resulting output Stokes vector is

$$\mathbf{S}_{out} = \mathbf{M}_D \cdot \mathbf{S}_{in}. \quad (9)$$

Since most photodetector elements are polarization insensitive, the output of the detector usually will be proportional to $s_{0,out}$, which can be written in vector form as

$$s_{0,out} = \mathbf{S}_D^T \cdot \mathbf{S}_{in} = m_{D,00}s_{0,in} + m_{D,01}s_{1,in} + m_{D,02}s_{2,in} + m_{D,03}s_{3,in}. \quad (10)$$

Equation (10) has four unknowns—the input Stokes parameters—so to solve for these unknowns, we must build up a system of linear equations like Eq. (10) using at least four different realizations of the diattenuation Stokes vector in Eq. (8). In matrix form, this system can be written as

$$\mathbf{X} = \begin{bmatrix} s_{0,out}^1 \\ s_{0,out}^2 \\ \vdots \\ s_{0,out}^N \end{bmatrix} = \begin{bmatrix} (\mathbf{S}_D^1)^T \\ (\mathbf{S}_D^2)^T \\ \vdots \\ (\mathbf{S}_D^N)^T \end{bmatrix} \cdot \mathbf{S}_{in} = \mathbf{A} \cdot \mathbf{S}_{in}. \quad (11)$$

The notation $(\mathbf{S}_D^i)^T$ represents the i th realization of the diattenuation Stokes vector. In general, the number of measurements $N \geq M$, where M is the number of dimensions that will be reconstructed in the polarimeter. The matrix \mathbf{A} in Eq. (11) is referred to as the system matrix, and its inverse is termed the data reduction matrix⁵ (DRM). We can estimate the unknown input Stokes vector as

$$\hat{\mathbf{S}}_{in} = \mathbf{A}^{-1} \cdot \mathbf{X}, \quad (12)$$

where the hat indicates that Eq. (12) is providing only an estimate. Sources of error could include noise in the measurement vector \mathbf{X} and calibration measurements in determining the DRM. Clearly we need to be careful about the selection of $(\mathbf{S}_D^i)^T$, as the condition number of the matrix \mathbf{A} must be low enough so that the inversion process is well behaved. More details are provided on this issue in the section on polarimeter optimization in Subsection 5.B.

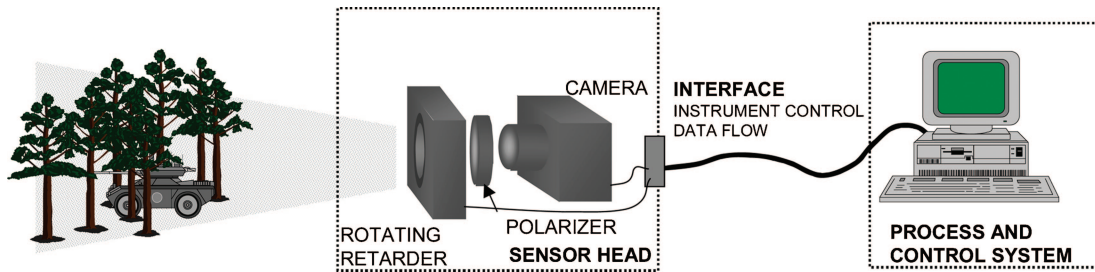


Fig. 3. (Color online) Polarimetric sensor using rotating polarization elements.

The DRM measurement strategy can be interpreted from a signal processing viewpoint.⁷⁷ Each of the entries in \mathbf{X} can be thought of as a projection of the unknown input Stokes vector onto an analysis vector $(\mathbf{S}_D^i)^T$. When $N = M$, the analysis vectors form a *nonorthogonal* basis in the conical space that is the allowed space of physically realizable Stokes vectors. When $N > M$, the analysis vectors form an overdetermined basis, or frame.⁷⁷ As discussed in Section 5, use of a frame can enhance the robustness of the measurement process.

B. Fourier Modulation Techniques

A common method of polarimetric measurement and data reduction is through the Fourier analysis of polarimetric signals. These methods were developed initially for Mueller and Jones matrix polarimeters for nonimaging measurement of polarized and partially polarized light^{42,78,79} and for ellipsometric measurements.^{80–82} They are readily generalized to spectral and imaging instruments.^{24,34,83,84}

In this approach, a series of images are acquired as the elements of the polarization state analyzer are varied in a harmonic fashion. The polarization of the incident light is encoded onto the harmonics of the detected signal. The Stokes-vector elements of the incident light are then recovered from a Fourier transform of the measured data set. The Stokes vector is computed independently for each pixel.

Consider a general polarimeter with incident light of unknown polarization and a PSA as shown schematically in Fig. 3. A series of N intensity measurements $s_{0,\text{out}}^n$ are made as in Subsection 3.A:

$$\mathbf{X} = \begin{bmatrix} s_{0,\text{out}}^1 \\ s_{0,\text{out}}^2 \\ \vdots \\ s_{0,\text{out}}^N \end{bmatrix} = \begin{bmatrix} (\mathbf{S}_D^1)^T \\ (\mathbf{S}_D^2)^T \\ \vdots \\ (\mathbf{S}_D^N)^T \end{bmatrix} \cdot \mathbf{S}_{\text{in}} = \mathbf{A} \cdot \mathbf{S}_{\text{in}}. \quad (13)$$

Varying the polarization elements of the analyzer modulates the analyzed polarization states. A typical method of varying the polarization elements is by rotating some or all of the elements in discrete steps. If the angular increments of the polarization elements are constant, only discrete frequencies are generated in the detected intensity \mathbf{X} , whose elements are written as x_n . The intensity x_n is collected for the n th position of the polarization elements in the PSA.

The detected signal can be written

$$x_n = \frac{b_0}{2} + \sum_{k=1}^{N-1} (b_k \cos k\theta_n + c_k \sin k\theta_n), \quad (14)$$

where the largest k is the highest frequency component in the signal and $\theta_n = n\theta$ is proportional to the angular frequency of the polarization element. The polarization content of the scene being imaged is encoded onto the various frequencies of the detected signal; i.e., the coefficients in the Fourier series expansion are functions of the incident Stokes vector. These relations are inverted to give the Stokes-vector elements in terms of the Fourier coefficients. The coefficients are determined from the set of intensities by a discrete Fourier transform,

$$\begin{aligned} b_0 &= \frac{1}{N} \sum_{n=0}^{N-1} x_n, \\ b_k &= \frac{2}{N} \sum_{n=0}^{N-1} i_n \cos\left(\frac{2nk\pi}{N}\right) = \sum_{n=0}^{N-1} i_n \cos(k\theta_n), \\ c_k &= \frac{2}{N} \sum_{n=0}^{N-1} i_n \sin\left(\frac{2nk\pi}{N}\right) = \sum_{n=0}^{N-1} i_n \sin(k\theta_n), \end{aligned} \quad (15)$$

where k is the harmonic, $\theta_n = n\Delta\theta$, and $\Delta\theta$ is the angular increment of the polarization elements. For N intensities, the coefficients for the $K = N/2$ harmonics are found. The step size of the rotation of the polarization element is determined by the number of measurements $\Delta\theta = 2\pi/N$.

The highest harmonic K in the polarimetric signal is determined from the analytical expression for the intensity written as a Fourier series. The minimum number of measurements N_{min} required to calculate the dc term and all cosine and sine (real and imaginary) terms in the Fourier transform is $N_{\text{min}} = 2K + 1$. It is often desirable to make more measurements than the minimum, or oversample, to help reduce the effects of noise. For oversampled data, the harmonics higher than the frequencies of the polarimetric signal are often used as diagnostic tools to indicate sources of systematic error.

The Fourier analysis of polarimetric signals provides several significant advantages for data reduction. First, if the analytical form is readily derived via a system Mueller matrix expression, this data reduction method is straightforward and computationally fast. Second, the system Mueller matrix may be parameterized such that diattenuation and retardance values and orientation of the elements may be deter-

mined in calibration. Third, this method often encompasses instruments where the elements are rotated continuously. In this case, the angular increment used for discrete steps of the rotated elements is replaced by the angular increment at which the next data acquisition is begun. Any motion of the element over the integration time of the sensor is compensated for in calibration. Fourth, the calculation of the discrete Fourier transform automatically gives a least-squares fit to the data. Finally, the discrete Fourier transform is a useful analytical tool for investigating many types of systematic error such as beam wander and linear drift. The susceptibility to harmful noise sources can be reduced through adjusting the parameters of measurements and the corresponding Fourier transform. More details of the effect of noise and errors on the measurements and ways to compensate or negate these effects are given in Refs. 85 and 86. The chief disadvantage of this approach is that the system Mueller matrix must be well known. In practice, this requires that the polarizers are pure diattenuators and the retarders are pure retarders; i.e., the polarizers contain no retardance and the retarders are not diattenuating.

C. Channeled Spectropolarimeters

Most polarization techniques that rely on retarding elements have to go to great lengths to develop a wave plate that has uniform retardance across the spectral range of interest. Efforts have been made to develop *achromatic retarders* in the visible and the IR spectra. Achromatic retarders are commercially available at visible wavelengths, but have only recently become available for infrared wavelengths.⁸⁷ When polarimetry and spectrometry are combined, the retardance can be calibrated wavelength by wavelength, reducing the problems associated with this effect.²⁷

Recent techniques have emerged that couple Fourier transform spectrometry with polarimetry to exploit the wavelength dependence of the retardance (in wavelengths) of high-order wave plates.⁷⁶ We assume that a wave plate of thickness L can be described by an index of refraction difference $\Delta n = n_e - n_o$, where n_e and n_o are the extraordinary and ordinary indices of refraction. We ignore dispersion in n over the wave band of interest for the purposes of this development. The phase difference induced between the radiation polarized parallel and perpendicular to the fast axis is given as

$$\delta = \frac{2\pi(\Delta n)L}{\lambda}. \quad (16)$$

When the thickness of the wave plate is chosen so that $\delta \gg 2\pi$, then the retardance varies rapidly as a function of the wavelength. The spectrum of the output intensity of the PSA is modulated in a manner analogous to Eq. (14). When the spectrum of this signal is measured with a Fourier transform spectrometer, the spectrum is modulated in a manner that depends on the polarization state. If the retard-

ers and PSA are designed carefully, and the spectrum of the incident signal is band limited, then spectrally distinct portions of the signal can be used to determine the Stokes parameters of interest.

It is essential that a Fourier transform spectrometer be used to make the spectral measurement. This is because the variation in retardance introduced by Eq. (16) provides a signal at spatial frequencies that correspond to wavelengths that are typically outside the spectral range of the detectors used. The method described by Oka and Kato⁷⁶ is not an imaging scheme. Sabatke *et al.*⁷⁴ developed a method to couple the channeled spectropolarimeter with a snapshot Fourier-based spectrometer to enable the instantaneous collection of spectral and polarimetric imagery information. This technique has been extended to several wave bands of interest.⁸⁸

Oka and Kaneko⁸⁹ introduced a novel and complimentary strategy for snapshot polarimeter when using monochromatic illumination. Whereas the channeled spectropolarimeter modulates the spectrum based on the polarization signature, the new method uses spatially varying thick retarders to spatially modulate the intensity image. The polarimetric features can be ideally reconstructed using a similar demodulation technique when the spatial Fourier spectrum of the scene is band limited.

4. Imaging Architecture for Integrated Polarimeters

There are several different approaches for polarimetric detection. As with spectral imaging where multi-dimensional data are acquired, the data acquisition process is a study in compromises. By the very nature of measuring polarization, multiple images are required to even partially characterize the polarization state of a scene. Since polarimetric data reduction manipulates the same pixel across multiple frames, any motion of the scene in the pixel results in artifacts that have the potential to mask the true polarization signature. Ideally, two spatial dimensions are desired, but due to this temporal image registration issue, the images must be acquired simultaneously or acquired as quickly as possible to minimize artifacts from platform or scene motion. The best solution for minimizing these artifacts is to acquire multiple images at the same time, but then the issue becomes spatial registration. Spatial registration of multiple images is complicated by the need to correct for both mechanical misalignment as well as optical "misalignment" arising from aberrations due to separate optical paths. Conceptually the simplest way to measure the polarization information is to use separate cameras with separate optics that are aligned to the same portion of the image (coboresighted). Early imaging polarimeters did this with both film and electronic cameras^{14,19} as well as scanning single-element photodetectors.⁹⁰ This strategy is difficult to execute properly, and has largely fallen out of favor. There are a number of integrated techniques that are used now. Trade-offs among these methods, as well as issues of cost and difficulty of fabrication and integration, are listed in Table 2.

Table 2. Comparison of Imaging Polarimetry Architectures

	Design Features	Fabrication–Integration Issues, Cost	Misregistration Issues
Rotating element	<ul style="list-style-type: none"> ● Robust ● Relatively small ● Not suitable for dynamic scenes 	<ul style="list-style-type: none"> ● Easiest to implement ● Inexpensive 	<ul style="list-style-type: none"> ● Scene and platform motion ● Beam wander not a problem or removed in software ● Misregistration is linear
Division of amplitude (multiple FPAs)	<ul style="list-style-type: none"> ● Simultaneous acquisition ● Large system size 	<ul style="list-style-type: none"> ● High mechanical flexibility and rigidity required ● Expensive ● Large 	<ul style="list-style-type: none"> ● Must register multiple FPAs ● Misregistration can be fixed ● Can be nonlinear
Division of aperture (single FPA)	<ul style="list-style-type: none"> ● Simultaneous acquisition ● Smaller size 	<ul style="list-style-type: none"> ● Loss of spatial resolution ● Expensive 	<ul style="list-style-type: none"> ● Fixed misregistration ● Can be nonlinear
Division of focal plane	<ul style="list-style-type: none"> ● Simultaneous acquisition ● Small and rugged ● Loss of spatial resolution 	<ul style="list-style-type: none"> ● Fabrication difficult ● Alignment difficult ● Very expensive 	<ul style="list-style-type: none"> ● IFOVs misregistered ● Requires interpolation ● Fixed registration
Coboresighted	<ul style="list-style-type: none"> ● Simultaneous acquisition ● Best used at long ranges 	<ul style="list-style-type: none"> ● Easy integration ● Expensive 	<ul style="list-style-type: none"> ● Misregistration not as stable

A. Division of Time Polarimeter

One commonly used approach is to rotate polarization elements in front of the camera system.^{16,20} This approach is attractive because it is relatively straightforward in both system design and data reduction. However, the obvious drawback is that both the scene and platform must be stationary to avoid introducing interframe motion. Figure 2 shows an example of the common rotating retarder polarimeter. In this type of polarimeter, the rotation of the polarization elements causes a modulation of the polarized light incident on the focal plane from the scene, and the data can be reconstructed using the methods discussed in Section 3. Reducing the data on a pixel-by-pixel basis produces Stokes images that can be used to produce images of the degree of linear polarization, degree of circular polarization, or other derived quantities such as orientation or ellipticity.

Most often the rotating element has been a polarizer. Only linear polarization states are detected in this approach. In addition, either the rotation rate in previous attempts has been too slow to achieve reasonable frame rates, or the polarizer was moved in steps with the imagery acquired between movements. Even with recent successes in continuously rotating the polarizer,⁸⁴ artifacts still remain if there is sufficient scene sensor movement during acquisition or if there is beam wander induced by the rotating element. Beam wander can result if there is a wedge in the rotating element or if the element wobbles in any sense. Nevertheless, if proper care is taken, the rotating element polarimeter can provide good results with a relatively small investment in hardware, design, and integration.

B. Division of Amplitude Polarimeters

DoAmP were first suggested and built by Garlick *et al.*¹⁴ for a two-channel system, then revived later for full-Stokes polarimeters,^{91,92} and have since been exploited by a number of authors. Figure 3 shows a full Stokes DoAmP polarimeter. This type of polar-

imeter consists of four separate focal-plane arrays. The camera system consists of four separate cameras mounted such that a single objective lens is used in combination with a series of polarizing beam splitters, retarders, and relay lenses to produce a polarimetric image. Rigid mechanical mounts are used to support the cameras in positions facing the four cube assembly exits. The polarizing beam-splitting cube assembly is used to balance the linear and circular measurements. The cameras simultaneously capture the four images necessary for computing a complete Stokes image, thus eliminating false polarization effects due to scene changes during the collection process.

In this particular example,⁹³ the polarimetric beam-splitter assembly is designed to measure the complete Stokes vector. The beam-splitting block includes three beam splitters, one 80/20 polarizing beam-splitting cube, two 50/50 polarizing beam-splitting cubes, and a quarter-wave and half-wave retarder. Each path through the beam-splitter block analyzes a different aspect of the incident polarization. This makes efficient use of the polarized light so that none of the light is absorbed or rejected. Furthermore, the analyzed polarization states are as nearly orthogonal as possible, and the analyzed states evenly span the possible incident polarization states.

As described in the first paragraph of Section 4, special care must be taken in alignment, and in practice, mechanical alignment to the required tolerances just is not possible. Further, the many degrees of freedom in the relay lens sets the result in different aberrations in each of the four channels. As a result, postprocessing is required to coregister the four images. One of the chief disadvantages is the size of the system with the four focal planes and the breadboard required to rigidly mount the focal planes and their optics. When full spatial resolution is desired and size and cost of components is less of an issue, this approach is suitable.

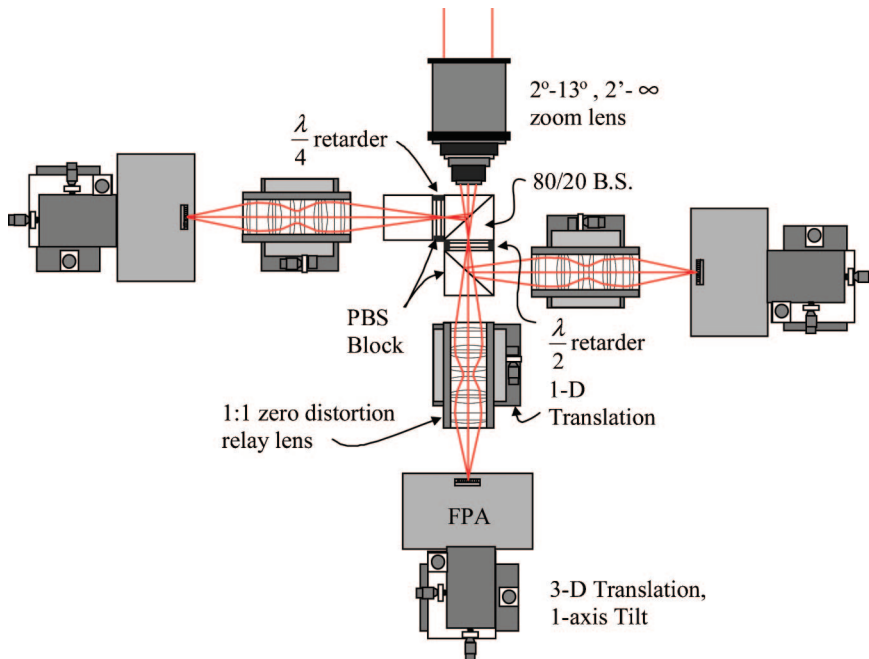


Fig. 4. (Color online) Division of amplitude polarimeter. The fourth camera is out of the plane of the page positioned above the PBS block after the quarter-wave retarder.

C. Division of Aperture Polarimeter

Figure 4 (Ref. 94) shows an architecture that can both acquire all of the polarization data simultaneously and ensure that the fields of view (FOVs) of all of the polarization channels are cobe-sighted. The architecture uses a single focal-plane array (FPA) and a reimaging system to project multiple images onto a FPA that are accurately coaligned. This architecture has the advantage that once the optics are mechanically fixed, the alignment has been shown to be stable in time when compared to DoAmP polarimeters. The improved stability is likely due to the longer optical paths that are typically necessary in DoAmP systems, translating small changes into larger deviations on the FPA. The architecture can be used both as a passive sensor (broadband illumination) and as an active monochromatic sensor. The primary disadvantages of the division of aperture polarimeter are the loss of spatial resolution (a factor of 2 in each linear dimension) and the volume and weight of

the additional reimaging optics. In addition, matching transmission, apodization, magnification, and distortion between the channels is difficult, but can be accomplished. It should also be noted that this strategy is more difficult to employ with coherent illumination due to coherent scattering and interference.

D. Division of Focal-Plane Array Polarimeters

The recent advances in FPA technology have led to the integration of micro-optical polarization elements directly onto the FPA.^{95,96} Most DoFP systems that have been made to date are only sensitive to linear polarization, though some discussion of full-Stokes DoFP systems has been raised.⁹⁷ An example system is shown in Fig. 5. DoFP systems have been manufactured for imaging in all regions of the optical spectrum, including visible,^{98,99} SWIR,¹ and LWIR.¹⁰⁰ Most DoFP systems have interlaced polarization superpixels as shown in Fig. 5, although some systems

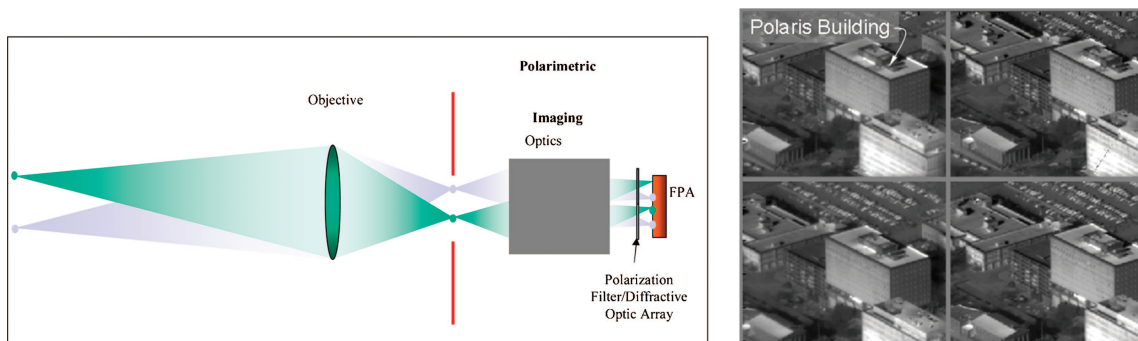


Fig. 5. (Color online) Division of aperture polarimeter and a raw focal plane image showing the four polarization channels. The four channels are reduced to polarization products such as DoLP. For this specific case, the four images are linearly polarized at 0°, 45°, 90°, and 135°.

have been made where the polarization information is sampled on a line-by-line basis.⁹⁸ A typical DoFP system will compute the Stokes vector at interpolation points in the FPA as indicated in Fig. 6. DoFP systems necessarily trade off spatial resolution for polarization information, as a 2×2 (or larger) convolution kernel must be applied to the image to estimate the Stokes vector at each point.

DoFP systems have the significant advantage that all polarization measurements are made simultaneously for every pixel in the scene. The component measurements that go into the Stokes-vector estimation are by construction coming from nearby points in the scene. However, the DoFP system by definition has pixel-to-pixel registration error in computing the Stokes vectors. The instantaneous fields of view (IFOVs) of adjacent pixels are (in principle) nonoverlapping, leading to exactly a 1-pixel registration error. The IFOV error can be partially mitigated by intentionally defocusing the optical point spread function, and recent efforts have been made to minimize the information loss while simultaneously minimizing IFOV error through interpolation.¹⁰⁰

5. System Considerations

A. Alignment and Calibration of Imaging Polarimeters

Alignment and calibration are important issues in acquiring polarimetric imagery, and knowledge of system characteristics is essential to obtaining good data. The authors have been involved in many measurement campaigns that, while qualitatively useful to those taking the data, cannot be used for quantitative analysis because of poor calibration. The credibility of reported results is dependent upon documented calibration procedures.

Each polarimetric system will have its own calibration and alignment issues, and it is not possible to summarize all possible scenarios here, or offer a prescription for handling these issues. We review general items that must be addressed and give examples of methods that have been used in the past to acquire data. System design will determine which methods might be relevant, and the designer must be ready to incorporate and justify the appropriate calibration and alignment procedures.

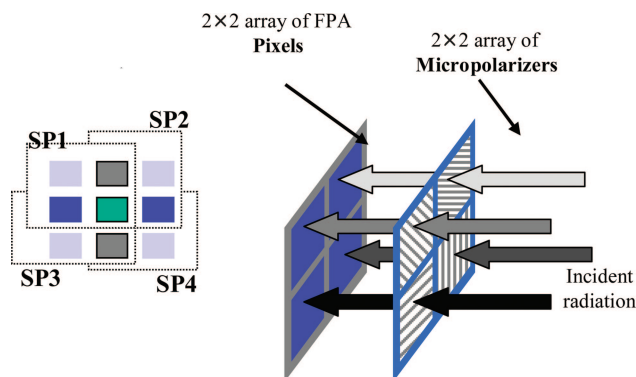


Fig. 6. (Color online) Division of focal plane polarimeter.

There are two calibration areas to be addressed: radiometric and polarimetric. The radiometric calibration determines the dynamic range of the detectors, ensures that the detectors are operated in a linear response region (or if not, guarantees that the response is known and consistent), and ensures that the detectors are not operated near their saturation points. If a detector array is used, and this will more than likely be the case for modern imaging systems, the response of individual detector elements must be known. A correction procedure for nonuniformities must be in place (e.g., a nonuniformity correction Naval Undersea Center look-up table).¹⁰⁰ These issues are no different from those facing the user of a nonpolarimetric system and will not be covered here. However, radiometric calibration is even more important to the final result because of the potential for inaccurate radiometry among channels to couple into and invalidate the polarimetric result. Polarimetric measurement issues that may need to be addressed include polarimetric system calibration, optical element polarimetric uniformity, optical axis alignment and optical element rotational alignment, and polarization aberrations.

Examples of polarimetric system calibration techniques are given in Azzam *et al.*¹⁰¹ and Goldstein and Chipman.¹⁰² The former contains a description of the calibration of the four-detector photopolarimeter where a simultaneous measurement of the Stokes vector is made. The latter concerns the calibration of a dual rotating retarder Mueller matrix polarimeter using Fourier data reduction techniques where time-sequential measurements are made. While neither of these are imaging systems, the approaches to calibration are instructive.

1. Experimental Determination of the Data Reduction Matrix

The DRM described in Section 3.A is estimated for an arbitrary polarimeter by measuring at least four linearly independent Stokes vectors that ideally form a maximum volume polyhedron inscribed inside the Poincaré sphere. When the number of measurements is exactly four, then the polyhedron is a regular tetrahedron.¹⁰¹ The equation that describes this measurement is similar to Eq. (12) and is given by

$$\mathbf{X} = \mathbf{A} \cdot \mathbf{S}, \quad (17)$$

where \mathbf{X} is a matrix of the measured intensities, \mathbf{S} is a matrix with columns that are input Stokes vectors, and \mathbf{A} is the instrument matrix. Each row of the instrument matrix is the analyzer vector for one measurement state of the instrument. Each column in \mathbf{X} is the response of all measurement (analyzer) states of the instrument to one calibration Stokes vector. The instrument matrix is then empirically calculated as

$$\mathbf{A} = \mathbf{X} \cdot \mathbf{S}^{-1}. \quad (18)$$

Clearly the calibration Stokes vectors that make up \mathbf{S} must be chosen so that the matrix is nonsingular. Measurements of unknown Stokes vectors may be made with the same measurement states used in the calibration once the instrument matrix \mathbf{A} is established. This approach is described elsewhere as a general formulation.⁵

2. Calibration of Fourier-Based Rotating Retarder Systems

In the rotating retarder system referenced in Subsection 2.F.1, the data reduction process is based on a Fourier analysis of the modulated signal that occurs when the retarders are rotated. Fourier coefficients are obtained as a function of Mueller matrix elements, and the equations are algebraically inverted. The Mueller matrix for the system is

$$\mathbf{M}_{\text{sys}} = \mathbf{P}_2 \mathbf{R}_2 \mathbf{M} \mathbf{R}_1 \mathbf{P}_1, \quad (19)$$

where \mathbf{M} is the Mueller matrix of the sample, \mathbf{R}_1 and \mathbf{R}_2 are the matrices for the retarders, and the \mathbf{P} are the matrices for the polarizers. The data collection process is allowed to proceed with no sample in place as a calibration. Since the Mueller matrix in the absence of a sample is the identity matrix, and expected and significant errors can be built into the data reduction equations (e.g., nonideal retarders and element orientation errors), these errors can be evaluated during calibration and used in sample data reduction. Note that for Mueller matrix systems, empty space or a high-quality mirror are good calibration samples. For Stokes systems, one has to be careful in the selection of calibration elements such as polarizers or retarders, and assumptions about the quality or properties of particular polarizers or retarders must be made with caution. Proper polarimetric measurement and calibration procedures can be a process of building up a simultaneous calibration of the polarimeter and the test signature so that the quality of the measurements made is better than the quality of the individual elements used. This is the case in both of the techniques just described.

3. Polarization Aberrations and Image Misalignment

An instantaneous FOV of the individual pixels may be an issue in polarization measurement, especially in imaging systems where the overall FOV of the system may be substantial.¹⁰³ This is an aspect of polarization aberrations,^{104,105} a subject that is independent of the classical wavefront aberrations more commonly studied in optics and that result from the differences created in amplitudes and phases as polarized light encounters interfaces.

Image registration, whether for sequential or simultaneous image collection, is a critical issue. Misregistration can result, for example, from separate focal planes that are not looking at the same region of space, or it can result from beam wander from a rotating element. Whatever the cause, Smith *et al.*¹⁰⁶ have suggested that images should be registered to 1/20 of a

pixel for acceptable polarimetric results. Ideally, the alignment should be mechanical. In practice, achieving even a half-pixel alignment mechanically can be difficult and software postprocessing alignment is frequently necessary.¹⁰⁷

B. Optimization

There have been significant research results recently concerning the optimization of passive and active polarimeter systems using both Fourier and DRM techniques. For passive DRM-based polarimeters, the estimate of the unknown incident Stokes vector is as given in Eq. (12). However, for real polarimeters, there are often many sources of uncertainty including, but not limited to, noise in the measurement process and calibration errors in determining the DRM. These error sources will be carried through the inversion of the DRM, leading to an error in the reconstructed Stokes vector. Consider first the case of measurement noise. If the DRM for the polarimeter is \mathbf{A} , but the measurement is

$$\mathbf{X} = \mathbf{A} \cdot \mathbf{S}_{\text{in}} + \mathbf{n}, \quad (20)$$

where \mathbf{n} is a noise vector, then we can define a measurement error

$$\vec{\varepsilon} = \hat{\mathbf{S}}_{\text{in}} - \mathbf{S}_{\text{in}} = \mathbf{A}^{-1} \cdot \mathbf{n}. \quad (21)$$

There are many potential metrics for quantifying the noise, and a detailed description of the trade-offs is presented by Ambirijan and Look¹⁰⁸ and Sabatke *et al.*,¹⁰⁹ but for the purposes of this discussion we will concentrate on the 2-norm of the DRM. If we assume that the noise is independent and identically distributed from pixel to pixel, then the 2-norm predicts the maximum length of the error vector in the reconstructed Stokes images as

$$\|\mathbf{A}\|_2 = \|\mathbf{A}^{-1}\|_2 = \sup_{\mathbf{n}} \frac{\|\mathbf{A}^{-1} \cdot \mathbf{n}\|_2}{\|\mathbf{n}\|_2} = \frac{\sup\|\vec{\varepsilon}\|_2}{\sqrt{N\sigma^2}}, \quad (22)$$

where σ^2 is the variance of the elements of the noise vector.

It has been shown that minimization of the 2-norm in Eq. (22) means that the $(\mathbf{S}_D)^T$ in Eq. (11) should be chosen to be maximally spaced on the surface of the Poincaré sphere¹⁰¹ so as to inscribe the maximum volume polyhedron within the Poincaré sphere as shown in Fig. 7. Satisfying the maximum volume condition also guarantees that the signal-to-noise ratio is equal in each of the three polarization channels s_1 , s_2 , and s_3 .^{77,110} When $N = 4$, this is a tetrahedron, but for larger values of N the geometrical shape has the appropriate number of corners. The value of making more than four measurements is that the overdetermined system in Eqs. (11) and (12) provides redundancy that increases the SNR by a factor of \sqrt{N} ,^{77,111,112} although reduction in noise can be made with a similar reduction in spatiotemporal

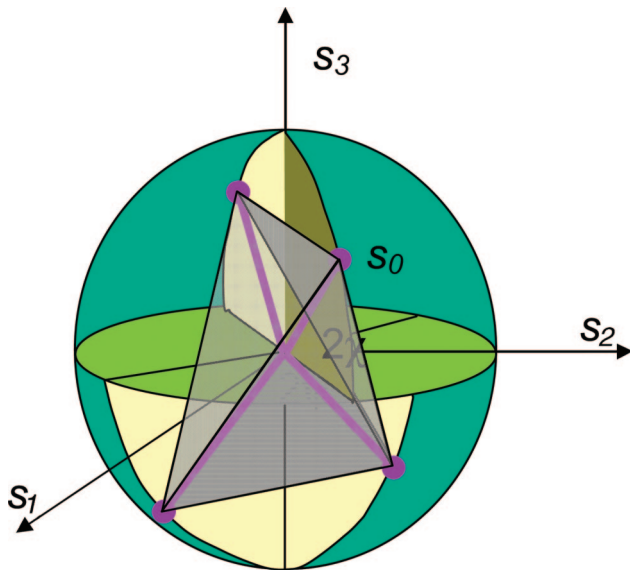


Fig. 7. (Color online) Optimal locations for measuring the polarization states are when the diattenuation vectors inscribe a regular tetrahedron inside the Poincaré sphere.

resolution by making four measurements and integrating for a longer time.¹¹¹ This optimization procedure was first carried out for rotating retarder polarimeters^{108,111–113} with the result that the common rotating quarter-wave plate polarimeter is suboptimal to a system composed of a rotating 132° wave plate, and that the optimum rotation angles for the fast axis of the wave plate (independent of retardance) are at $\pm 15.1^\circ$ and $\pm 51.6^\circ$ with respect to the orientation of the linear polarization analyzer. Similar optimization studies have been performed for linear polarization,¹¹⁴ dual rotating retarder,¹¹³ variable retardance,^{77,110} arbitrary-state polarimeters,¹⁰¹ and dual rotating retarder Mueller polarimeters.¹¹⁵ A number of experimental validation studies exist that demonstrate the value of using an optimized polarimeter.^{27,109,111,112,116}

In addition to noise considerations, there are usually calibration errors associated with the experimental determination of the DRM \mathbf{A} . In this case, we can recast Eq. (11) as

$$\mathbf{X} = (\mathbf{A} + \Delta) \cdot \mathbf{S}_{in}, \quad (23)$$

where Δ is the calibration error matrix. In this case, Eq. (12) becomes

$$\vec{\varepsilon} = \mathbf{A}^{-1} \Delta \cdot \mathbf{S}_{in}, \quad (24)$$

which tells us that the error is a function of the calibration error and the input Stokes vector.¹¹⁷ Equation (24) implies that polarimeter optimization is not as straightforward as simply optimizing the condition number of the DRM. The effects of Eq. (24) are analyzed by Tyo⁷⁷ for a rotating retarder polarimeter, and found that the optimum polarimeter with respect to Eq. (24) is not the optimum polarimeter with re-

spect to Eq. (22). For other classes of polarimeters, Eq. (24) can be used to find the best setting of parameters to provide minimum error.

6. Conclusions

The sensing of optical polarization information for remote sensing is an historically underused technique. In many applications, polarization phenomena are ignored, and the optical field is treated as scalar. While this can be reasonably accurate in many scenarios, it is clear that the ability to measure polarization information, especially across a scene, provides additional information that can be exploited. Imaging polarimetry is an emerging technique that promises to enhance many fields of optical metrology ranging from remote sensing to atmospheric sciences to industrial monitoring.

In this paper, we have discussed many of the important developments in imaging polarimetry. We have attempted to survey the literature, and we have provided a general overview of most of the strategies that can be employed for various tasks. A subject such as imaging polarimetry would be adequately covered in a much longer work, but we refer the reader to the extensive reference list that provides much greater detail on the topics discussed herein. We have attempted to focus on “first” discussions of topics where possible, and have necessarily left out many relevant references throughout. However, an interested reader can follow through the references provided to get a more complete picture of the state of the literature.

Imaging polarimetry is a field rich with potential for future work. Advances are needed in sensor technology, data-retrieval and analysis algorithms, and applications. While much has been accomplished in recent years, there is still a need for sensor systems with improved accuracy, precision, and stability. Particularly useful would be better and more complete quantification of these characteristics for currently existing and future systems. This implies a need for improved calibration techniques and more widely accepted and followed characterization procedures. For example, current technology makes use of Mueller matrix images, as promoted by Chipman,¹¹⁸ a practical way of characterizing polarization elements and systems. There is also a significant opportunity for creative ideas in dealing with the temporal and spatial trade-offs that presently exist in imaging polarimetry. And, finally, as the technology advances, there is a great variety of applications waiting to be addressed with imaging polarimetry.

References

1. C. S. L. Chun, D. L. Fleming, and E. J. Torok, “Polarization-sensitive, thermal imaging,” in *Automatic Object Recognition IV*, F. A. Sadjadi, ed., Proc. SPIE **2234**, 275–286 (1994).
2. R. C. Jones, “A new calculus for the treatment of optical systems: I. Description and discussion of the calculus,” *J. Opt. Soc. Am.* **31**, 488–493 (1941).
3. S.-Y. Lu and R. A. Chipman, “Interpretation of Mueller ma-

- trices based on the polar decomposition," *J. Opt. Soc. Am. A* **13**, 1106–1113 (1996).
4. W. R. Shurcliff, *Polarized Light* (Harvard U. Press, 1966).
 5. R. A. Chipman, "Polarimetry," in *Handbook of Optics* (McGraw-Hill, 1995), Vol. 2, Chap. 22.
 6. G. G. Stokes, "On the composition and resolution of streams of polarized light from different sources," *Trans. Cambridge Philos. Soc.* **9**, 399–416 (1852).
 7. D. F. J. Arago and A. J. Fresnel, "On the action of rays of polarized light upon each other," *Ann. Chim. Phys.* **3**, 288 (1819); reprinted in *The Wave Theory of Light, Memories by Huygens, Young, and Fresnel*, Henry Crew, ed. (American Book, 1900).
 8. D. F. J. Arago, *Ann. Chim. Phys.* **1**, 89 (1824).
 9. R. A. Millikan, "A study of the polarization of the light emitted by incandescent solid and liquid surfaces. I," *Phys. Rev.* **3**, 81–99 (1895).
 10. R. A. Millikan, "A study of the polarization of the light emitted by incandescent solid and liquid surfaces. II," *Phys. Rev.* **3**, 177–192 (1895).
 11. O. Sandus, "A review of emission polarization," *Appl. Opt.* **4**, 1634–1642 (1965).
 12. J. L. Johnson, *Infrared Polarization Signature Feasibility Tests*, Repts. TR-EO-74-1 and ADC00113 (U.S. Army Mobility Equipment Research and Development Center, 1974).
 13. S. A. Chin-Bing, *Infrared Polarization Signature Analysis*, Rep. ADC008418 (Defense Technical Information Center, 1976).
 14. G. F. J. Garlick, G. A. Steigmann, and W. E. Lamb, "Differential optical polarization detectors," U.S. patent 3,992,571 (16 November 1976).
 15. R. Walraven, "Polarization imagery," in *Optical Polarimetry: Instrumentation and Applications*, R. M. A. Azzam and D. L. Coffeen, eds., *Proc. SPIE* **112**, 164–167 (1977).
 16. R. Walraven, "Polarization imagery," *Opt. Eng.* **20**, 14–18 (1981).
 17. J. E. Solomon, "Polarization imaging," *Appl. Opt.* **20**, 1537–1544 (1981).
 18. D. L. Coffeen, "Polarization and scattering characteristics in the atmospheres of Earth, Venus, and Jupiter," *J. Opt. Soc. Am.* **69**, 1051–1064 (1979).
 19. K. L. Coulson, V. S. Whitehead, and C. Campbell, "Polarized views of the Earth from orbital altitude," in *Ocean Optics VIII*, M. A. Blizard, ed., *Proc. SPIE* **637**, 35–41 (1986).
 20. W. G. Egan, W. R. Johnson, and V. S. Whitehead, "Terrestrial polarization imagery obtained from the space shuttle: characterization and interpretation," *Appl. Opt.* **30**, 435–442 (1991).
 21. T. Prosch, D. Hennings, and E. Raschke, "Video polarimetry: a new imaging technique in atmospheric science," *Appl. Opt.* **22**, 1360–1363 (1983).
 22. J. O. Stenflo and H. Povel, "Astronomical polarimeter with 2D detector arrays," *Appl. Opt.* **24**, 3893–3898 (1985).
 23. J. L. Pezzaniti and R. A. Chipman, "Imaging polarimeters for optical metrology," in *Polarimetry: Radar, Infrared, Visible, Ultraviolet, and X-Ray*, R. A. Chipman and J. W. Morris, eds., *Proc. SPIE* **1317**, 280–294 (1990).
 24. J. L. Pezzaniti and R. A. Chipman, "Mueller matrix imaging polarimetry," *Opt. Eng.* **34**, 1558–1568 (1995).
 25. G. Vane and A. F. H. Goetz, "Terrestrial imaging spectroscopy," *Remote Sens. Environ.* **24**, 1–29, (1988).
 26. J. A. Shaw, "Degree of linear polarization in spectral radiances from water-viewing infrared polarimeters," *Appl. Opt.* **38**, 3157–3165 (1999).
 27. J. S. Tyo and T. S. Turner, "Variable retardance, Fourier transform imaging spectropolarimeters for visible spectrum remote sensing," *Appl. Opt.* **40**, 1450–1458 (2001).
 28. L. J. Cheng, J. C. Mahoney, and G. Reyes, "Target detection using an AOTF hyperspectral imager," in *Optical Pattern Recognition V*, D. P. Casasent and T. Chao, eds., *Proc. SPIE* **2237**, 251–259 (1994).
 29. S. Q. Duntley, "Underwater visibility and photography," in *Optical Aspects of Oceanography*, N. G. Jerlov, ed. (Academic, 1974), pp. 138–149.
 30. G. D. Gilbert and J. C. Pernicka, "Improvement of underwater visibility by reduction of backscatter with a circular polarization technique," in *Underwater Photo-Optics I*, A. B. Dember, ed., *Proc. SPIE* **7**, A-III-1–A-III-10 (1966).
 31. J. S. Tyo, M. P. Rowe, E. N. Pugh, and N. Engheta, "Target detection in optically scattering media by polarization-difference imaging," *Appl. Opt.* **35**, 1855–1870 (1996).
 32. M. P. Silverman and W. Strange, "Object delineation within turbid media by backscattering of phase modulated light," *Opt. Commun.* **144**, 7–11 (1997).
 33. S. G. Demos and R. R. Alfano, "Optical polarization imaging," *Appl. Opt.* **36**, 150–155 (1997).
 34. D. B. Chenault and J. L. Pezzaniti, "Polarization imaging through scattering media," in *Polarization Measurement, Analysis, and Remote Sensing III*, D. B. Chenault, M. J. Duggin, W. G. Egan, and D. H. Goldstein, eds., *Proc. SPIE* **4133**, 124–133 (2000).
 35. P. C. Y. Chang, J. G. Walker, K. I. Hopcraft, B. Ablitt, and E. Jakeman, "Polarization discrimination for active imaging in scattering media," *Opt. Commun.* **159**, 1–6 (1999).
 36. G. D. Lewis, D. L. Jordan, and P. J. Roberts, "Backscattering target detection in a turbid medium by polarization discrimination," *Appl. Opt.* **38**, 3937–3944 (1999).
 37. B. A. Swartz and J. D. Cummings, "Laser range-gated underwater imaging including polarization discrimination," in *Underwater Imaging, Photography, and Visibility*, R. W. Spinrad, ed., *Proc. SPIE* **1537**, 42–56 (1991).
 38. S. G. Demos, H. B. Radousky, and R. R. Alfano, "Deep subsurface imaging in tissues using spectral and polarization filtering," *Opt. Express* **7**, 23–28 (2000).
 39. J. S. Tyo, "Improvement of the point spread function in scattering media by polarization difference imaging," *J. Opt. Soc. Am. A* **17**, 1–10 (2000).
 40. S. G. Demos and R. R. Alfano, "Temporal gating in highly scattering media by the degree of optical polarization," *Opt. Lett.* **21**, 161–163 (1996).
 41. R. A. Chipman, "Polarization diversity active imaging," in *Image Reconstruction and Restoration II*, T. J. Schulz, ed., *Proc. SPIE* **3170**, 68–73 (1997).
 42. R. M. A. Azzam, "Photopolarimetric measurement of the Mueller matrix by Fourier analysis of a single detected signal," *Opt. Lett.* **2**, 148–150 (1978).
 43. P. Clémenceau, S. Breugnot, and L. Collot, "Polarization diversity active imaging," in *Laser Radar Technology and Applications III*, G. W. Kamerman, ed., *Proc. SPIE* **3380**, 284–291 (1998).
 44. L. Le Hors, P. Hartemann, and S. Breugnot, "Multispectral polarization active imager in the visible band," in *Laser Radar Technology and Applications V*, G. W. Kamerman, U. N. Singh, C. Werner, V. V. Molebny, eds., *Proc. SPIE* **4035**, 380–389 (2000).
 45. S. Breugnot and P. Clémenceau, "Modeling and performances of a polarization active imager at $\lambda = 806$ nm," *Opt. Eng.* **39**, 2681–2688 (2000).
 46. P. Réfrégier and F. Goudail, "Invariant polarimetric contrast parameters of coherent light," *J. Opt. Soc. Am. A* **19**, 1223–1233 (2002).
 47. P. Réfrégier, F. Goudail, and N. Roux, "Estimation of the degree of polarization in active coherent imagery by using the natural representation," *J. Opt. Soc. Am. A* **21**, 2292–2300 (2004).
 48. J. S. Baba, J.-R. Chung, A. H. DeLaughter, B. D. Cameron, and

- G. L. Cote, "Development and calibration of an automated Mueller matrix polarization imaging system," *J. Biomed. Opt.* **7**, 341–349 (2002).
49. J. Wolfe and R. A. Chipman, "High-speed imaging polarimeter," in *Polarization Science and Remote Sensing*, J. A. Shaw and J. S. Tyo, eds., Proc. SPIE **5158**, 24–32 (2003).
 50. M. Mujat, E. Baleine, and A. Dogariu, "Interferometric imaging polarimeter," *J. Opt. Soc. Am. A* **21**, 2244–2249 (2004).
 51. T. Sakai, T. Nagai, M. Nakazato, Y. Mano, and T. Matsumura, "Ice clouds and Asian dust studied with lidar measurements of particle extinction-to-backscatter ratio, particle depolarization, and water-vapor mixing ratio over Tsukuba," *Appl. Opt.* **42**, 7103–7116 (2003).
 52. J. M. Intrieri, M. D. Shupe, T. Uttal, and B. J. McCarty, "An annual cycle of Arctic cloud characteristics observed by radar and lidar at SHEBA," *J. Geophys. Res.* **107**, SHE5-1–SHE5-15 (2002).
 53. K. Sassen, "The polarization lidar technique for cloud research: a review and current assessment," *Bull. Am. Meteorol. Soc.* **72**, 1848–1866 (1991).
 54. J. A. Reagan, M. P. McCormick, and J. D. Spinhime, "Lidar sensing of aerosols and clouds in the troposphere and stratosphere," *Proc. IEEE* **77**, 433–448 (1989).
 55. J. E. Kalshoven, Jr. and P. W. Dabney, "Remote sensing of the Earth's surface with an airborne polarized laser," *IEEE Trans. Geosci. Remote Sens.* **31**, 438–446 (1993).
 56. S. Tan and R. M. Narayanan, "Design and performance of a multiwavelength airborne polarimetric lidar for vegetation remote sensing," *Appl. Opt.* **43**, 2360–2368 (2004).
 57. J. H. Chumside, J. J. Wilson, and V. V. Tatarskii, "Airborne lidar for fisheries applications," *Opt. Eng.* **40**, 406–414 (2001).
 58. N. L. Seldomridge, J. A. Shaw, and K. S. Repasky, "Dual-polarization lidar using a liquid crystal variable retarder," *Opt. Eng.* (to be published).
 59. K. P. Bishop, H. D. McIntire, M. P. Fetrow, and L. McMackin, "Multispectral polarimeter imaging in the visible to near IR," in *Targets and Backgrounds: Characterization and Representation V*, W. R. Watkins, D. Clement, and W. R. Reynolds, eds., Proc. SPIE **3699**, 49–57 (1999).
 60. K. Voss and Y. Liu, "Polarized radiance distribution measurements of skylight I: system description and characterization," *Appl. Opt.* **36**, 6083–6094 (1997).
 61. J. North and M. Duggin, "Stokes vector imaging of the polarized sky-dome," *Appl. Opt.* **36**, 723–730 (1997).
 62. G. Horvath, A. Barta, J. Gal, B. Suhai, and O. Haiman, "Ground-based full-sky imaging polarimetry of rapidly changing skies and its use for polarimetric cloud detection," *Appl. Opt.* **41**, 543–559 (2002).
 63. N. J. Pust and J. A. Shaw, "Dual-field imaging polarimeter using liquid crystal variable retarders," *Appl. Opt.* **45**, 5470–5478 (2006).
 64. D. Lemke, F. Garzon, H. Gemuend, U. Groezinger, I. Heinrichsen, U. Klaas, W. Kraetschmer, E. Kreysa, P. Luetzow-Wentzky, J. Schubert, M. Wells, and J. Wolf, "ISOPHOT: far-infrared imaging, polarimetry, and spectrophotometry on Infrared Space Observatory," in *Infrared Spaceborne Remote Sensing*, M. S. Scholl, ed., Proc. SPIE **2019**, 28–33 (1993).
 65. R. S. Loe and M. J. Duggin, "Hyperspectral imaging polarimeter design and calibration," in *Polarization Analysis, Measurement, and Remote Sensing IV*, D. H. Goldstein, D. B. Chenault, W. G. Egan, and M. J. Duggin, eds., Proc. SPIE **4481**, 195–205 (2002).
 66. D. A. Glenar, J. J. Hillman, B. Saif, and J. Bergstralh, "Acousto-optic imaging spectropolarimetry for remote sensing," *Appl. Opt.* **33**, 7412–7424 (1994).
 67. W. M. Smith and K. M. Smith, "A polarimetric spectral imager using acousto-optic tunable filters," *Exp. Astron. A* **1**, 329–343 (1991).
 68. L. J. Denes, M. Gottlieb, B. Kaminsky, and P. Metes, "AOTF polarization difference imaging," in *27th AIPR Workshop: Advances in Computer-Assisted Recognition*, R. J. Mericks, ed., Proc. SPIE **3584**, 106–115 (1999).
 69. N. Gupta, R. Dahmani, and S. Choy, "Acousto-optic tunable filter based visible-to-near-infrared spectropolarimetric imager," *Opt. Eng.* **41**, 1033–1038 (2002).
 70. N. S. Prasad, "An acousto-optic tunable filter based active, long-wave IR spectropolarimetric imager," in *Chemical and Biological Standoff Detection*, J. O. Jensen and J.-M. Theriault, eds., Proc. SPIE **5268**, 104–112 (2004).
 71. G. L. Jensen and J. Q. Peterson, "Hyperspectral imaging polarimeter in the infrared," in *Infrared Spaceborne Remote Sensing VI*, M. Strojnik and B. F. Andresen, eds., Proc. SPIE **3437**, 42–51 (1998).
 72. S. H. Jones, F. J. Iannarilli, and P. L. Kebebian, "Realization of quantitative-grade fieldable snapshot imaging spectropolarimeter," *Opt. Express* **12**, 6559–6573 (2004).
 73. F. J. Iannarilli, J. A. Shaw, S. H. Jones, and H. E. Scott, "Snapshot LWIR hyperspectral polarimetric imager for ocean surface sensing," in *Polarization Analysis, Measurement, and Remote Sensing III*, D. B. Chenault, M. J. Duggin, W. G. Egan and D. H. Goldstein, eds., Proc. SPIE **4133**, 270–283 (2000).
 74. D. Sabatke, A. Locke, E. L. Dereniak, M. Descour, J. Garcia, T. Hamilton, and R. W. McMillan, "Snapshot imaging spectropolarimeter," *Opt. Eng.* **41**, 1048–1053 (2002).
 75. D. Goldstein, *Polarized Light* (Dekker, 2003).
 76. K. Oka and T. Kato, "Spectroscopic polarimetry with a channeled spectrum," *Opt. Lett.* **24**, 1475–1477 (1999).
 77. J. S. Tyo, "Design of optimal polarimeters: maximization of signal-to-noise ratio and minimization of systematic errors," *Appl. Opt.* **41**, 619–630 (2002).
 78. P. S. Hauge, "Mueller matrix ellipsometry with imperfect compensators," *J. Opt. Soc. Am. A* **68**, 1519–1528 (1978).
 79. R. M. A. Azzam, "A simple Fourier photopolarimeter with rotating polarizer and analyzer for measuring Jones and Mueller matrices," *Opt. Commun.* **25**, 137–140 (1978).
 80. P. S. Hauge and F. H. Dill, "A rotating-compensator Fourier ellipsometer," *Opt. Commun.* **14**, 431–437 (1975).
 81. L. Y. Chen and D. W. Lynch, "Scanning ellipsometer by rotating polarizer and analyzer," *Appl. Opt.* **26**, 5221–5228 (1987).
 82. D. E. Aspnes, "Photometric ellipsometer for measuring partially polarized light," *J. Opt. Soc. Am. A* **65**, 1274–1278 (1975).
 83. S. Y. Brezhna, I. V. Bereznyy, and M. Takashi, "Dynamic photometric imaging polarizer-sample analyzer polarimeter," *J. Opt. Soc. Am. A* **18**, 666–707 (2001).
 84. J. S. Harchanko, D. B. Chenault, C. F. Farlow, and K. Spradley, "Detecting a surface swimmer using long wave infrared imaging polarimetry," in *Photonics for Port and Harbor Security*, M. J. DeWeert and T. T. Saito, eds., Proc. SPIE **5780** (2005).
 85. D. H. Goldstein and R. A. Chipman, "An error analysis of a Mueller matrix polarimeter," *J. Opt. Soc. Am. A* **7**, 693–700 (1990).
 86. D. B. Chenault, J. L. Pezzaniti, and R. A. Chipman, "Mueller matrix polarimeter algorithms," in *Polarization Analysis and Measurement*, Proc. SPIE **1746**, 231–246 (1992).
 87. D. B. Chenault and R. A. Chipman, "Infrared birefringence spectra for cadmium sulfide and cadmium selenide," *Appl. Opt.* **32**, 4223–4227 (1993).
 88. N. Hagan, A. Locke, D. Sabatke, E. Dereniak, and D. Sass, "Methods and applications of snapshot spectropolarimetry," in *Polarization: Measurement, Analysis, and Remote Sensing*

- VII, D. H. Goldstein and D. Chenault, eds., Proc SPIE **5432**, 167–174 (2004).
89. K. Oka and T. Kaneko, "Compact complete imaging polarimeter using birefringent wedge prisms," *Opt. Express* **11**, 1510–1519 (2003).
 90. J. Halaijan and H. Hallock, "Principles and techniques of polarimetric mapping," in *Proceedings of the Eighth International Symposium on Remote Sensing of Environment (ERIM, 1972)*, Vol. 1, pp. 523–540.
 91. R. M. A. Azzam, "Arrangement of four photodetectors for measuring the state of polarization of light," *Opt. Lett.* **10**, 309–311 (1985).
 92. J. D. Barter, P. H. Y. Lee, and H. R. Thompson, "Stokes parameter imaging of scattering surfaces," in *Polarization: Measurement, Analysis, and Remote Sensing*, D. H. Goldstein and R. A. Chipman, eds., Proc. SPIE **3121**, 314–320 (1997).
 93. C. A. Farlow, D. B. Chenault, K. D. Spradley, M. G. Gulley, M. W. Jones, and C. M. Persons, "Imaging polarimeter development and application," in *Polarization Analysis and Measurement IV*, D. H. Goldstein, D. B. Chenault, W. Egan, and M. J. Duggin, eds., Proc. SPIE **4819**, 118–125 (2001).
 94. J. L. Pezzaniti and D. B. Chenault, "A division of aperture MWIR imaging polarimeter," in *Polarization Science and Remote Sensing II*, J. A. Shaw and J. S. Tyo, eds., Proc. SPIE **5888** (2005).
 95. D. M. Rust, "Integrated dual imaging detector," U.S. patent 5,438,414 (1 August 1995).
 96. A. G. Andreau and Z. K. Kalayjian, "Polarization imaging: principles and integrated polarimeters," *IEEE Sens. J.* **2**, 566–576 (2002).
 97. G. P. Nordin, J. T. Meier, P. C. Deguzman, and M. Jones, "Diffractive optical element for Stokes vector measurement with a focal plane array," in *Polarization Measurement, Analysis, and Remote Sensing II*, D. H. Goldstein and D. B. Chenault, eds., Proc. SPIE **3754**, 169–177 (1999).
 98. C. K. Harnett and H. G. Craighead, "Liquid-crystal micropolarizer for polarization-difference imaging," *Appl. Opt.* **41**, 1291–1296 (2002).
 99. L. B. Wolff and A. G. Andreau, "Polarization camera sensors," *Image Vis. Comput.* **13**, 497–510 (1995).
 100. J. K. Boger, J. S. Tyo, B. M. Ratliff, M. P. Fetrow, W. Black, and R. Kumar, "Modeling precision and accuracy of a LWIR microgrid array imaging polarimeter," in *Polarization Science and Remote Sensing II*, J. A. Shaw and J. S. Tyo, eds., Proc. SPIE **5888** (2005).
 101. R. M. A. Azzam, I. M. Elminyawi, and A. M. El-Saba, "General analysis and optimization of the four-detector photopolarimeter," *J. Opt. Soc. Am. A* **5**, 681–689 (1988).
 102. D. H. Goldstein and R. A. Chipman, "Error analysis of a Mueller matrix polarimeter," *J. Opt. Soc. Am. A* **7**, 693–700 (1990).
 103. R. A. Chipman, "Polarization analysis of optical systems," *Opt. Eng.* **28**, 90–99 (1989).
 104. J. P. McGuire and R. A. Chipman, "Polarization aberrations. 1. Rotationally symmetric optical systems," *Appl. Opt.* **33**, 5080–5100 (1994).
 105. J. P. McGuire and R. A. Chipman, "Polarization aberrations. 2. Tilted and decentered optical systems," *Appl. Opt.* **33**, 5101–5107 (1994).
 106. M. H. Smith, J. B. Woodruff, and J. D. Howe, "Beam wander considerations in imaging polarimetry," in Proc. SPIE **3754**, 50–54 (1999).
 107. C. M. Persons and D. B. Chenault, "Automated registration of polarimetric imagery using Fourier transform techniques," in *Polarization: Measurement, Analysis, and Remote Sensing V*, D. L. Goldstein and D. B. Chenault, eds., Proc. SPIE **4819**, 107–117 (2002).
 108. A. Ambirajan and D. C. Look, "Optimum angles for a polarimeter: part I," *Opt. Eng.* **34**, 1651–1655 (1995).
 109. D. S. Sabatke, A. M. Locke, M. R. Descour, W. C. Sweatt, J. P. Garcia, E. Dereniak, S. A. Kemme, and G. S. Phipps, "Figures of merit for complete Stokes polarimeters," in *Polarization Analysis, Measurement, and Remote Sensing III*, D. B. Chenault, M. J. Duggin, W. G. Egan, and D. H. Goldstein, eds., Proc. SPIE **4133**, 75–81 (2000).
 110. J. S. Tyo, "Noise equalization in Stokes parameter images obtained by use of variable retardance polarimeters," *Opt. Lett.* **25**, 1198–2000 (2000).
 111. D. S. Sabatke, M. R. Descour, E. Dereniak, W. C. Sweatt, S. A. Kemme, and G. S. Phipps, "Optimization of retardance for a complete Stokes polarimeter," *Opt. Lett.* **25**, 802–804 (2000).
 112. V. A. Dlugunovich, V. N. Snopko, and A. V. Tsaruk, "Minimizing the measurement error of the Stokes parameters when the setting angles of a phase plate are varied," *J. Opt. Technol.* **67**, 797–800 (2000).
 113. A. Ambirajan and D. C. Look, "Optimum angles for a polarimeter: part II," *Opt. Eng.* **34**, 1656–1659 (1995).
 114. J. S. Tyo, "Optimum linear combination strategy for a N -channel polarization sensitive vision or imaging system," *J. Opt. Soc. Am. A* **15**, 359–366 (1998).
 115. M. H. Smith, "Optimization of a dual-rotating-retarder Mueller matrix polarimeter," *Appl. Opt.* **41**, 2488–2495 (2002).
 116. V. A. Dlugunovich, V. N. Snopko, and A. V. Tsaruk, "Analysis of a method for measuring polarization characteristics with a Stokes polarimeter having a rotating phase plate," *J. Opt. Technol.* **68**, 269–273 (2001).
 117. P. Li and J. S. Tyo, "Experimental measurement of optimal polarimeter systems," in *Polarization Science and Remote Sensing*, J. A. Shaw and J. S. Tyo, eds., Proc. SPIE **5158**, 103–112 (2003).
 118. R. A. Chipman, College of Optical Sciences, University of Arizona, Tucson, Arizona 85721 (personal communication, 2006).